Analysis of the Magnetic Field Homogeneity for an Equilateral Triangular Helmholtz Coil

Andres F. Restrepo*, Edinson Franco, Hector Cadavid, and Carlos R. Pinedo

Abstract—This paper presents a mathematical analysis of the magnetic field homogeneity for an Equilateral Triangular Helmholtz (ETH) coil. The magnetic field analysis is based on the Biot-Savart law in which a Taylor series approximation is performed to obtain the analytical distance that complies with the Helmholtz condition between the pair of coils. This is done to compare the magnetic field distributions of the ETH and the Circular Helmholtz (CH) coils for the parameters side length $(2a, \sqrt{3}a)$ and radius (a) respectively. Furthermore, an approximate expression of the magnetic field homogeneity with regard to the side length parameter is obtained and finally a computational model of the ETH coil using COMSOL® is performed in order to validate the calculated and experimental results. The results show that the ETH coils have a lower magnetic field homogeneity than the CH coils for the described parameters, and the implementation of either one basically depends on the application specifications.

1. INTRODUCTION

The controlled and homogeneous magnetic fields have several uses in different areas of knowledge such as bioelectromagnetics [1, 2], electromagnetic compatibility [3], shielding [4], etc. Stimulating biological systems via magnetic fields demand a uniform magnetic field generation [5, 6] which may guarantee a completely controlled and continuous exposure to the biological material being studied [7]. The systems commonly used to generate uniform magnetic fields are based on permanent magnets and air-core coils of simple geometrical shapes [8, 9] (circular, square and rectangular), of two or more coils [10, 11] with different distances between each other [12].

The Helmholtz pair is one of the most frequently used configurations in applications of electromagnetic stimulation, due to the generation of highly uniform magnetic fields [14], in addition to applications of measurement and compensation of magnetic fields [7, 15]. Recently, arrangements with Helmholtz coils from single axis to multiple axes [16] are used in applications of controlled drug delivery [17] and electromagnetic navigation [18, 19] using micro-robots and/or magnetic particles [20].

The circular and square coils are the most implemented geometries in the building of systems to generate uniform magnetic fields, based on the Helmholtz configuration [21]. Therefore, the design parameters for circular and square Helmholtz coils are firmly well-defined in the literature [6, 13, 24], supported by mathematical analysis and computational models [12]. However, Al-Sowayan [22] proposed a design with equilateral triangular coils in a Helmholtz configuration and found a relationship between separation distance and side length through simulation. This paper presents a mathematical analysis to determine the separation distance related to the side length, to ensure the Helmholtz condition between a pair of equilateral triangular coils. Furthermore, the homogeneity of the magnetic field distribution generated by this pair is compared with the one generated by a Circular Helmholtz (CH) coil [24]. The ratio between the magnetic field distribution and the physical parameters of the radiation system will give way for a faster more reliable design keeping the application specifications in mind.

2. DESCRIPTION OF THE UNIFORM MAGNETIC FIELD GENERATION SYSTEMS

The Biot-Savart law [21] was used to analyze the magnetic field generated by the Helmholtz coils, for any given electric current. The Helmholtz coil setup consists of two equally spaced coils h placed on each side of a common axis (x, y or z), generating a uniform magnetic field in the area of interest. Both coils are connected in a series circuit, where each coil contains N number of conductive thread turns and carry an electric current I.
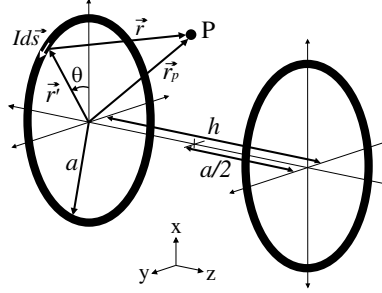

Figure 1. Configuration of the CH coil.

2.1. CH Coil

Considering the Biot-Savart law for the configuration of Fig. 1, the generated magnetic field (B) at point P in Cartesian coordinate, due to an individual circular coil [23], can be calculated as shown in Equation (1) [24]; where $d\vec{s}$ is an infinitesimal segment of the current loop, μ_0 is the permeability of the free space, r is the distance from the infinitesimal segment of the current loop to P, r_p is the distance from the origin to P and r' is the distance from the origin to the infinitesimal segment of the current loop.

$$\vec{B}(x,y,z) = \frac{\mu_0}{4\pi} \oint \frac{I d\vec{s} \times \vec{r}}{|\vec{r}|^3} = B_x \hat{i} + B_y \hat{j} + B_z \hat{k} \tag{1}$$

$$B_x = a B_{Z0} \int_0^{2\pi} z \cos\theta \frac{d\theta}{F_z^{3/2}}$$

$$B_y = a B_{Z0} \int_0^{2\pi} z \sin\theta \frac{d\theta}{F_z^{3/2}}$$

$$B_z = a B_{Z0} \int_0^{2\pi} (a - x\cos\theta - y\sin\theta) \frac{d\theta}{F_z^{3/2}}$$

where

$$F_z = z^2 + (x - a*\cos\theta)^2 + (y - a*\sin\theta)^2$$

$$B_{Z0} = \frac{\mu_0 NI}{4\pi}$$

Given Equation (1), the magnetic field generated by the CH coil on z-direction is calculated by the following Equation (2):

$$\vec{B}(z) = \frac{\mu_0 NIa^2}{2} \left[\frac{1}{\left(a^2 + \left(z + \frac{h}{2}\right)^2\right)^{3/2}} + \frac{1}{\left(a^2 + \left(z - \frac{h}{2}\right)^2\right)^{3/2}} \right] \tag{2}$$

The separation distance h that complies with the Helmholtz condition for the circular coils is equal to its radius a ($h = a$) [25]. Therefore, the magnetic field along the z axis in Equation (2) can be approximated, by Taylor series representation, as the magnetic field on the segment $| z | \leq a/2$. The approximate expression is presented in the equation below:

$$B_z(z)|_{|z| \leq a/2} \approx \frac{8\mu_0 NI}{5\sqrt{5}a} \left[1 - \frac{144}{125}\left(\frac{z}{a}\right)^4 \right] \tag{3}$$

Solving Equation (3), the effect of the term $(z/a)^4$ is practically negligible for the interval $| z | \leq a/2$. Therefore, the resulting magnetic field $B_z(z)$ is an almost constant function around $z = 0$ and the magnetic field distribution is uniform with an associated homogeneity.

2.2. ETH Coil

Considering $2a$ as the side length of the equilateral triangular coil that is shown in Fig. 2(a), where b ($b_1 = a/\sqrt{3}$) is the perpendicular distance from each side of the coil to the origin, a similar analysis to the circular coil is performed. Therefore, the magnetic field at point P in Cartesian coordinate, due to an individual equilateral triangular coil, can be calculated as shown in Equation (4), where $\vec{dl}$ is an infinitesimal segment of the current loop, s is the perpendicular distance from the current loop axis to P, r is the distance from an extreme of the current loop to P, $\hat{r}$ is a unit vector and finally θ_o and θ_f are the angles formed from the current loop axis to the projection lines from the extremes of the current loop to P respectively.
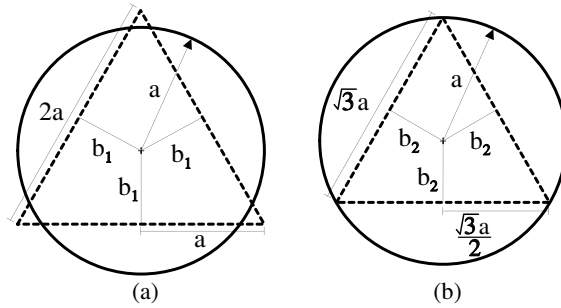

Figure 2. Relation between radius a of the circular coil and side length of the equilateral triangular coil: (a) Side length $2a$. (b) Side length $\sqrt{3}a$.

$$\vec{B}(x, y, z) = B_{Z0} \sum_{i=1}^{3} \int_{\theta_{o_i}}^{\theta_{f_i}} \frac{\sin\theta}{s_i} d\theta = B_x \hat{i} + B_y \hat{j} + B_z \hat{k} \tag{4}$$

$$\begin{bmatrix} B_x \\ B_y \\ B_z \end{bmatrix} = B_{Z0} \begin{bmatrix} -\frac{1}{2}z & z & -\frac{1}{2}z \\ -\frac{\sqrt{3}}{2}z & 0 & \frac{\sqrt{3}}{2}z \\ y_1' + \frac{a}{\sqrt{3}} & -x + \frac{a}{\sqrt{3}} & -y_3' + \frac{a}{\sqrt{3}} \end{bmatrix} * \begin{bmatrix} F_1 \\ F_2 \\ F_3 \end{bmatrix}$$

where

$$F_{1,3} = \frac{1}{s_{1,3}^2} \left(\frac{x_{1,3}' + a}{\sqrt{(x_{1,3}' + a)^2 + s_{1,3}^2}} - \frac{x_{1,3}' - a}{\sqrt{(x_{1,3}' - a)^2 + s_{1,3}^2}} \right)$$

$$F_2 = \frac{1}{s_2^2} \left(\frac{y + a}{\sqrt{(y + a)^2 + s_2^2}} - \frac{y - a}{\sqrt{(y - a)^2 + s_2^2}} \right)$$

$$s_{1,3} = \sqrt{(y'_{1,3} \pm a/\sqrt{3})^2 + z^2}$$

$$s_2 = \sqrt{(x - a/\sqrt{3})^2 + z^2}$$

The resulting magnetic field on each coordinate axis is the sum of the contributions of the magnetic field generated by each equilateral triangular coil. The analysis of sides 1 and 3 is performed rotating each plane xy (with respect to the z axis) an angle α, in this case $\mp 30°$, obtaining new coordinate systems (x'_1, y'_1, z) and (x'_3, y'_3, z) respectively. The matrix of rotation is shown in the following Equation (5):

$$\begin{bmatrix} x' \\ y' \\ z \end{bmatrix} = \begin{bmatrix} \cos\alpha & \sin\alpha & 0 \\ -\sin\alpha & \cos\alpha & 0 \\ 0 & 0 & 1 \end{bmatrix} * \begin{bmatrix} x \\ y \\ z \end{bmatrix} \tag{5}$$
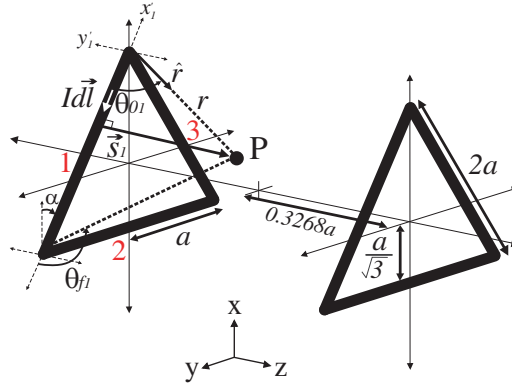

Figure 3. Configuration of the ETH coil.

Considering Equation (4), the magnetic field of the Equilateral Triangular Helmholtz (ETH) coil (Fig. 3) on the z-direction is calculated by the following equation:

$$\vec{B}_z(z) = \frac{\sqrt{3}\mu_0 N I a^2}{2\pi} \left[\frac{1}{\left(\frac{a^2}{3} + \left(z + \frac{h}{2}\right)^2\right)\left(\frac{4a^2}{3} + \left(z + \frac{h}{2}\right)^2\right)^{1/2}} + \frac{1}{\left(\frac{a^2}{3} + \left(z - \frac{h}{2}\right)^2\right)\left(\frac{4a^2}{3} + \left(z - \frac{h}{2}\right)^2\right)^{1/2}} \right] \tag{6}$$

Separation distance h in Equation (6) can be found satisfying the uniformity condition by Taylor series expansion [13]. By symmetry around $z = 0$, $B_z(z)$ is an even function which ensures that all their odd derivatives are zero (for example $dB_z/dz(0) = 0$). The second derivative is suppressed to zero $(\partial^2 B_z/\partial z^2(0) = 0)$ in order to reach a homogeneous magnetic field on the central region of the ETH coil (uniformity condition), thus we arrive to the following equation:

$$\left(a^2 + 3\left(\frac{h}{2}\right)^2\right)\left(\frac{a^2}{3} + \left(\frac{h}{2}\right)^2\right)\left(\frac{4a^2}{3} + \left(\frac{h}{2}\right)^2\right) - \left(\frac{h}{2}\right)^2\left(a^2 + \left(\frac{h}{2}\right)^2\right)\left(\frac{19a^2}{3} + 7\left(\frac{h}{2}\right)^2\right) = 0 \tag{7}$$

Replacing $x = a^2$ and $y = (h/2)^2$ into Equation (7) results in:

$$(4/9)x^3 - (10/3)x^2 y - (22/3)xy^2 - 4y^3 = 0 \tag{8}$$

The previous equation may be simplified even more by calculating the linear factor of the expression $y - kx$, then placing $y = kx$ into Equation (8), which will result in:

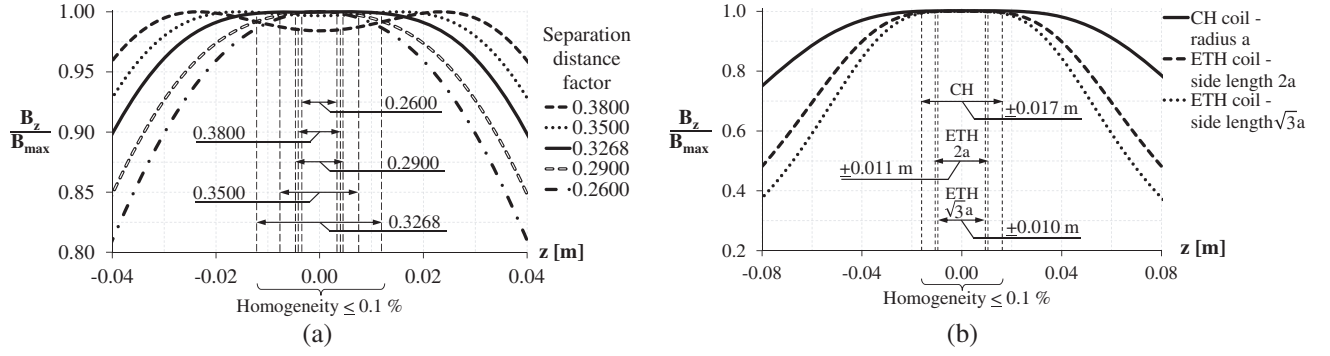$$4k^3 + (22/3)k^2 + (10/3)k - (4/9) = 0 \tag{9}$$

Figure 4. Normalized magnetic field distributions: (a) Equilateral triangular coils at different separation distances. (b) CH and ETH coils comparison.

A real number of $k = 0.1068$ after solving the polynomial in Equation (8) was obtained. Therefore, the separation distance h of the ETH coil is obtained as shown in the following equation:

$$\frac{h}{2} = 0.3268a \tag{10}$$

The curves obtained in this paper (calculated, simulated and experimental data) for the circular and equilateral triangular coils were performed considering the following parameters $a = 0.1\,\mathrm{m}$, $N = 50$ and $I = 1\,\mathrm{A}$. The calculated separation distance in Equation (10) is replaced in Equation (6) to obtain the magnetic field on the z axis, and it is compared by evaluating different separation distances for a pair of equilateral triangular coils with a side length $2a$ as shown in Fig. 4(a), where the normalized magnetic fields $(B_z/B_{\max})$ related to the distance along the z axis are shown.

Figure 4(a) shows the regions with uniform magnetic field (homogeneity $\leq 0.1\%$) for different separation distance factors, concluding that the separation distance factor (0.3268) calculated in Equation (10) has the largest area with a uniform magnetic field along the z axis for the same value of homogeneity $\leq 0.1\%$. Now, the approximate expressions of the magnetic field at the center of the ETH coil in Equation (11) and the fourth derivative in Equation (12) of $B_z(z)$ (both evaluated at $z = 0$) are calculated in order to reach the approximate expression by Taylor series:

$$B_z(0) \approx \frac{9\mu_0 NI}{1.3204\pi\sqrt{4.3204}a} \tag{11}$$

$$\frac{\partial^4 B_z}{\partial z^4}(0) \approx -24\left(\frac{9\mu_0 NI}{1.3204\pi\sqrt{4.3204}a}\right)\left(\frac{6.0254}{a^4}\right) \tag{12}$$

Finally, replacing Equations (11) and (12) in the Taylor series expansion [13] around $z = 0$ ($h = 0.6536a$), the magnetic field $B_z(z)$ generated by the ETH coil is obtained for the range $|z| \leq 0.3268a$:

$$B_z(z)\big|_{|z|\leq 0.3268a} \approx \frac{9\mu_0 NI}{1.3204\pi\sqrt{4.3204}a}\left[1 - 6.0254\left(\frac{z}{a}\right)^4\right] \tag{13}$$

Considering a reduction in the side length $\sqrt{3}a$ of the equilateral triangular coils [22] where $b_2 = a/2$ (Fig. 2(b)), the magnitude of the resultant magnetic field B_z increases according to Equation (6) and the magnetic field distribution has a reduction of the homogeneity as shown in Fig. 4(b), where the normalized magnetic fields $(B_z/B_{\max})$ related to the z axis for the CH [13] and ETH coils are presented. Fig. 4(b) illustrates the CH coil has a greater homogeneity than the ETH coil for the cases $2a$ and $\sqrt{3}a$.

3. MAGNETIC FIELD HOMOGENEITY OF THE ETH COIL

The magnetic field variability within a defined space [26] can be measured and represented as the magnetic field homogeneity (H). This variation is usually expressed as a percentage difference (%) of

the magnetic fields around the central region, as it is manifested in the equation below:

$$H[\%] = \frac{|B(x,y,z) - B(0,0,0)|}{|B(0,0,0)|} * 100 \tag{14}$$

The values and volumes which seem to be most commonly used to specify magnetic field homogeneity are $\pm 0.1\%$, $\pm 0.5\%$ and $\pm 1\%$ for cylindrical, spherical or cubic distributions [24]. This parameter H depends on the requirements of the application, therefore it is necessary to find a relationship between the physical parameters of the Helmholtz coil and the magnetic field homogeneity in the volume of interest.

By replacing Equations (2) and (6) into Equation (14) a relationship between a given length (along the z axis) with a uniform magnetic field and the parameter a of the coils can be obtained (radius for CH coils or half of the side length for ETH coils). However, the complete analytical solution of Equation (14) is very complex. A possible solution could be to evaluate different values of z and obtain the ratio $|z/a|$ for particular homogeneities H_z.

In addition, the expressions of the magnetic field obtained by Taylor series expansion in the ranges $|z| \le a/2$ and $|z| \le 0.3268a$ in Equations (3) and (13) for the CH and ETH coils respectively, giving way for an approximate ratio $|z/a|$ [13] as presented in the equations below:

$$|z/a| \leqslant 0.305 * H_z^{1/4} \tag{15}$$

$$|z/a| \leqslant 0.202 * H_z^{1/4} \tag{16}$$

Table 1 shows the solutions of the ratio $|z/a|$, for specific homogeneities H_z, obtained from Equation (14) evaluating different values of z and that obtained from the approximate expressions (15) and (16) for CH and ETH coils respectively. These relationships allow to verify that the circular geometry has a greater homogeneity than the equilateral triangular geometry in a Helmholtz configuration, given that for the same values H_z and a, the circular configuration generates a greater length with an axial uniform magnetic field on the z-direction.

Table 1. Comparison of the ratios $|z/a|$ for CH and ETH coils.

Homogeneity	CH coil		ETH coil	
(H_z)	$|z/a|$	$|z/a|$ approx.	$|z/a|$	$|z/a|$ approx.
$< 0.01\%$	≤ 0.097	≤ 0.096	≤ 0.064	≤ 0.064
$< 0.02\%$	≤ 0.115	≤ 0.115	≤ 0.076	≤ 0.076
$< 0.05\%$	≤ 0.145	≤ 0.144	≤ 0.096	≤ 0.096
$< 0.1\%$	≤ 0.173	≤ 0.172	≤ 0.115	≤ 0.114
$< 0.2\%$	≤ 0.206	≤ 0.204	≤ 0.137	≤ 0.135
$< 0.5\%$	≤ 0.262	≤ 0.256	≤ 0.173	≤ 0.170
$< 1\%$	≤ 0.314	≤ 0.305	≤ 0.207	≤ 0.202
$< 2\%$	≤ 0.378	≤ 0.363	≤ 0.250	≤ 0.240
$< 5\%$	≤ 0.488	≤ 0.456	≤ 0.323	≤ 0.302
$< 10\%$	≤ 0.602	≤ 0.542	≤ 0.398	≤ 0.359

4. COMPUTATIONAL MODEL OF THE ETH COIL

The analysis of magnetic field uniformity of the ETH coil was done via a 3D computational model, which was built using COMSOL Multiphysics®, to be able to verify the magnetic field distribution based on the finite element method (FEM) for solving Maxwell's equations through simulation and the AC/DC Module for static and low frequency magnetic field analysis [12, 13]. Each equilateral triangular coil

was characterized as a solid conductive material powered by an electric current without considering the eddy-current effects. The physical and electrical parameters such as side length, separation distance, resistivity and electric current among others are the most important simulation parameters for the ETH coil [13].

Figure 5 provides the computational model and the simulation results of the magnetic flux density of the ETH coil with a side length $2a$, considering the parameters a, N and I described above. In Fig. 5(a) the direction of the magnetic field lines and the magnetic field distribution over the central region are presented, whilst Fig. 5(b) shows the contour map of the magnetic flux density in millitesla (mT) units.
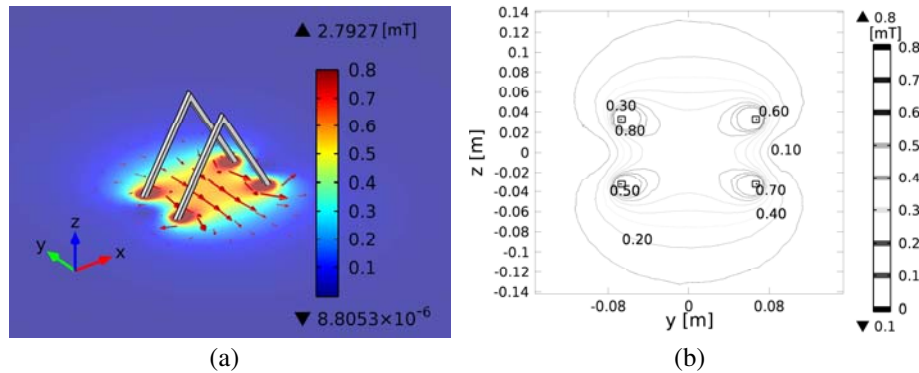

(a)   (b)

Figure 5. Simulation of the magnetic flux density of the ETH coil: (a) Computational model. (b) Contour map.

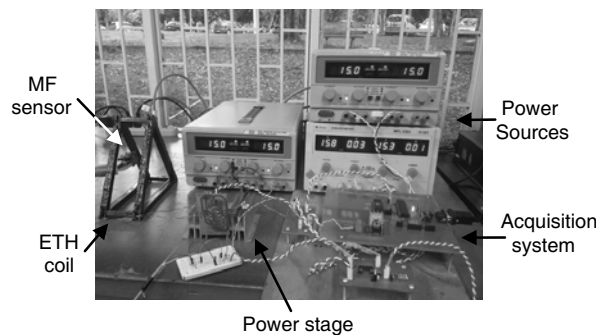**Figure 6.** Experimental setup of the ETH coil.
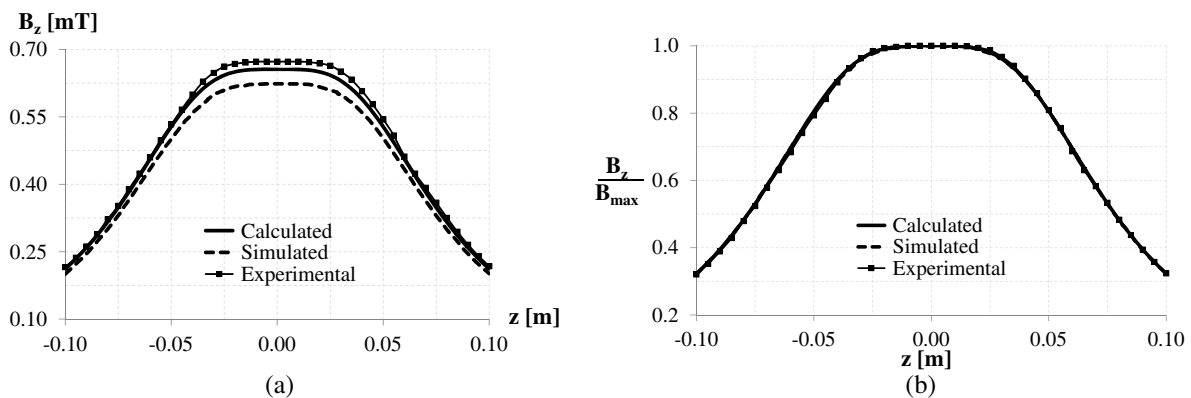

(a)   (b)

Figure 7. Magnetic field distributions of the ETH coil with a side length $2a$: (a) Non-normalized magnetic field. (b) Normalized magnetic field.

The experimental results were obtained using an acquisition system based on the AD22151 Hall effect sensor [13] for measuring the magnetic field distribution, the complete experimental setup of the ETH coil is shown in Fig. 6 where it also shows the power stage, power sources etc. In order to validate the computational model of the ETH coil, the magnetic field along the z axis ($x = y = 0$) is obtained by simulation, and the results are compared with the calculated Equation (6) and experimental data. Fig. 7 shows the magnetic field distributions generated by the ETH coil with a side length $2a$.

In Fig. 7(a) the simulated and experimental results are compared to the calculated data of the magnetic fields along the center of the ETH coil ($| z | \leq 0.3268a$) where maximum errors of 4.9% and 2.6% were established respectively. Meanwhile, Fig. 7(b) shows a good correlation of the normalized magnetic fields, where maximum errors of 0.7% and 1.8% were presented for simulated and experimental results in comparison to the calculated data respectively. The obtained simulation error could be due to the selected parameters and assumptions like numerical method, boundary conditions, magnetic properties and geometry of the wire and coiling [13].

5. CONCLUSION

The ETH coils have a lower magnetic field homogeneity than the CH coils for the parameters side length $(2a, \sqrt{3}a)$ and radius (a) respectively. The ETH coils emerge as an alternative for the generation systems of extremely low frequency (ELF) magnetic fields and its choice basically depends on the applications and constraints such as the working volume, power consumption, accuracy, etc. Furthermore, the ratio between the desired homogeneity and the side length of the ETH coil obtained by Taylor series approximation allows a quick design depending on the requirements of the application.

ACKNOWLEDGMENT

REFERENCES

1. De Seze, R., A. Lahitte, J. M. Moreau, and B. Veyret, "Generation of extremely-low frequency magnetic fields with standard available commercial equipment: Implications for experimental bioelectromagnetics work," *Bioelectrochem. Bioenerg.*, Vol. 35, No. 1–2, 127–131, 1994.
2. Farina, M., M. A. Mariggio, T. Pietrangelo, J. J. Stupak, A. Morini, and G. Fano, "ELF-EMFs induced effects on cell lines: Controlling ELF generation in laboratory," *Progress In Electromagnetics Research B*, Vol. 24, 131–153, 2010.
3. Satav, S. M. and V. Agarwal, "Design and development of a low-cost digital magnetic field meter with wide dynamic range for EMC precompliance measurements and other applications," *IEEE Trans. Instrum. Meas.*, Vol. 58, No. 8, 2837–2846, 2009.
4. Forte, G. O., G. Farrher, L. R. Canali, and E. Anoardo, "Automatic shielding-shimming magnetic field compensator for excluded volume applications," *IEEE Trans. Control Syst. Technol.*, Vol. 18, No. 4, 976–983, 2010.
5. Schuderer, J., W. Oesch, N. Felber, D. Spät, and N. Kuster, "In vitro exposure apparatus for ELF magnetic fields," *Bioelectromagnetics*, Vol. 25, No. 8, 582–591, 2004.
6. Alamgir, A. K., J. Fang, C. Gu, and Z. Han, "Square Helmholtz coil with homogeneous field for magnetic measurement of longer HTS tapes," *Physica C: Superconductivity*, Vol. 424, No. 1–2, 17–24, 2005.
7. Martino, C. F., L. Portelli, K. McCabe, M. Hernandez, and F. Barnes, "Reduction of the Earths magnetic field inhibits growth rates of model cancer cell lines," *Bioelectromagnetics*, Vol. 31, No. 8, 649–655, 2010.

8. Kirschvink, J. L., "Uniform magnetic fields and double-wrapped coil systems: Improved techniques for the design of bioelectromagnetic experiments," *Bioelectromagnetics*, Vol. 13, No. 5, 401–411, 1992.

9. Nouri, N. and B. Plaster, "Comparison of magnetic field uniformities for discretized and finite-sized standard cos, solenoidal, and spherical coils," *Nucl. Instr. Meth. Phys. Res. A*, Vol. 723, 30–35, 2013.

10. Pittman, M. E. and D. L. Waidelich, "Three and four coil systems for homogeneous magnetic fields," *IEEE Trans. Aerosp.*, Vol. 2, No. 1, 36–45, 1964.

11. Herceg, D., A. Juhas, and M. Milutinov, "A design of a four square coil system for a biomagnetic experiment," *Facta Universitatis Series: Electronics and Energetics*, Vol. 22, No. 3, 285–292, 2009.

12. Azpúrua, M. A., "A semi-analytical method for the design of coil-systems for homogeneous magnetostatic field generation," *Progress In Electromagnetics Research B*, Vol. 37, 171–189, 2012.

13. Restrepo, A. F., E. Franco, and C. R. Pinedo, "A design and implementation methodology of a system to generate uniform magnetic field volume with tri-axial square Helmholtz coils," *Inf. Tecnol.*, Vol. 25, No. 2, 3–14, 2014.

14. Haghnegahdar, A., H. Khosrovpanah, A. Andisheh-Tadbir, G. Mortazavi, M. Saeedi, S. M. Mortazavi, A. Zamani, M. Haghani, M. Shojaei, H. Parsaei, and O. Koohi, "Design and fabrication of Helmholtz coils to study the effects of pulsed electromagnetic fields on the healing process in periodontitis: Preliminary animal results," *J. Biomed. Phys. Eng.*, Vol. 4, No. 3, 83–90, 2014.

15. Enoki, S., T. Asahi, S. Watanabe, T. Mizuno, and K. Takeshita, "Electromagnetic measurement of the rail displacement by two triangular coils," *IEEE Trans. Magn.*, Vol. 38, No. 5, 3303–3305, 2002.

16. Choi, H., S. Jeong, C. Lee, B. Park, S. Ko, J.-O. Park, and S. Park, "Three-dimensional swimming tadpole mini-robot using three-axis Helmholtz coils," *Int. J. Control Autom.*, Vol. 12, No. 3, 662–669, 2014.

17. Hossain, A. B., M. H. Cho, and S. Y. Lee, "Magnetic nanoparticle density mapping from the magnetically induced displacement data: A simulation study," *Biomed. Eng. Online*, Vol. 11, No. 1, 13, 2012.

18. Cao, Q., X. Han, B. Zhang, and L. Li, "Analysis and optimal design of magnetic navigation system using Helmholtz and Maxwell coils," *IEEE Trans. Appl. Supercond.*, Vol. 22, No. 3, 4401504, 2012.

19. Go, G., H. Choi, S. Jeong, C. Lee, S. Y. Ko, J.-O. Park, and S. Park, "Electromagnetic navigation system using simple coil structure (4 coils) for 3-D locomotive microrobot," *IEEE Trans. Magn.*, Vol. 51, No. 4, 1–7, 2015.

20. Ha, Y. H., B. H. Han, and S. Y. Lee, "Magnetic propulsion of a magnetic device using three square-Helmholtz coils and a square-Maxwell coil," *Med. Biol. Eng. Comput.*, Vol. 48, No. 2, 139–145, 2010.

21. Bell, G. B. and A. A. Marino, "Exposure system for production of uniform magnetic fields," *Journal of Bioelectricity*, Vol. 8, No. 2, 147–158, 1989.

22. Al-Sowayan, S., "Generation of homogenous magnetic field using equilateral triangular coils.," *Int. J. Appl. Eng. Res.*, Vol. 9, No. 1, 137–143, 2014.

23. Kdzia, P., T. Czechowski, M. Baranowski, J. Jurga, and E. Szcześniak, "Analysis of uniformity of magnetic field generated by the two-pair coil system," *Appl. Magn. Reson.*, Vol. 44, No. 5, 605–618, 2013.

24. Beiranvand, R., "Analyzing the uniformity of the generated magnetic field by a practical one-dimensional Helmholtz coils system," *Rev. Sci. Instrum.*, Vol. 84, No. 7, 075109, 2013.

25. Restrepo, A. F., L. J. Martinez, C. R. Pinedo, E. Franco, and H. Cadavid, "Design study for a cellular culture bioreactor coupled with a magnetic stimulation system," *IEEE Lat. Am. T.*, Vol. 11, No. 1, 130–136, 2013.

26. Wang, J., S. She, and S. Zhang, "An improved Helmholtz coil and analysis of its magnetic field homogeneity," *Rev. Sci. Instrum.*, Vol. 73, No. 5, 2175–2179, 2002.